





CHEMICAL TECHNOLOGY

Article

Received: 11 January 2023 | Revised: 04 May 2023 |
Accepted: 10 May 2023 | Published online: 29 May 2023

UDC 544.7+543.5

<https://doi.org/10.31489/2959-0663/2-23-3>

Toufik Chouchane^{1*} , Atmane Boukari¹, Ouahida Khireddine¹ ,
Sana Chibani¹ , Sabiha Chouchane² 

¹Research Center in Industrial Technologies CRTI, Algiers, Algeria;
²Faculty of Sciences, Badji Mokhtar Annaba University, Annaba, Algeria
(*Corresponding author's e-mail: t.chouchane@crti.dz)

Cu(II) Removal from Aqueous Medium Using Blast Furnace Slag (BFS) as an Effective Adsorbent

The copper adsorption by blast furnace slag (BFS) in an aqueous medium was considered based on the influencing parameters, namely the agitation speed, pH, temperature, the particle size of the solid, and the initial concentration. Physicochemical studies have shown that BFS is consisted mainly from SiO₂, CaO, Al₂O₃, and MgO with a specific surface area of 238 m²/g. Under the optimum parameters, the maximum adsorption amount at equilibrium (140 min) corresponds to 45.16 mg/g. Exploration of adsorption isotherms revealed that the Langmuir model is more consistent with the experimental data. The values of the Freundlich (*n*) and Langmuir (*RL*) parameters indicate that the adsorption is favorable. On the other hand, the values of Temkin (*bt*) and Redlich-Peterson (*g*) parameters show that adsorption is physical. Pseudo-second order of the adsorption process was confirmed using a kinetic study. Moreover, the diffusional study specified that the transfer of copper from the solution to BFS is successively controlled by external and intraparticle diffusion. The thermodynamic parameters showed that the adsorption of Cu(II) on BFS was feasible, spontaneous, exothermic, and less entropic. The desorption phenomenon has revealed that BFS can be reused for three consecutive cycles.

Keywords: blast furnace slag, copper, adsorption in batch mode, adsorption isotherm, adsorption kinetics, desorption, depollution.

Introduction

Water pollution by metal ions is one of the most undesirable environmental problems in the world that requires immediate solutions [1–4]. Indeed, with the multiplication of inhabitants, the expansion of urbanization, and the development of industries, natural water sites have become discharges of toxic industrial pollutants [5, 6]. For this reason, it is necessary to proceed with the elimination of toxic elements from water through reliable, efficient, and rigorous treatments such as membrane technology [7], chemical precipitation [8], ion-exchange [9] and adsorption [10]. Among these used processes, the adsorption phenomenon is often considered as the most optimal, since it is effective, easy to implement and less expensive [11, 12].

In this context, we set out to develop a simple and effective process of depollution by adsorption phenomenon. Blast furnace slag from the steel complex El-Hadjar Annaba, Algeria was chosen as a low-cost adsorbent. Besides, copper was chosen as the metal pollutant.

BFS is a by-product of the metallurgical steel industry resulting from the production of cast iron in blast furnaces. The annual production of slag in the world is very high, which constitutes a serious ecological problem and a loss of important financial resources [13].

According to the literature, slag and its derivatives as effective adsorbents have been the subject of many studies, especially in cases of the adsorption of metal ions [14, 15], phosphorus [16, 17] and dyes [18, 19]. Copper is reputed as a dangerous and toxic element, due to the fact that it accumulates over time and, in addition, is not biodegradable [20]. These parameters represent a significant risk factor for humans and their environment [21]. Therefore, its removal is inevitable and more than necessary. The presence of various adsorbents used in the process of copper removal in an aqueous medium is noted in the literature, namely carbon-based adsorbents [22], clay minerals [23], and agricultural adsorbents [24].

The main purpose of this study is the valorization of blast furnace slag in the field of adsorption of metal ions in solution. The slag treatment, the kinetic study, the adsorbate/adsorbent interaction, the nature of the process, and the desorption capacity will contribute to the evaluation of BFS as an adsorbent.

Analysis by XRF and XRD were used for the physicochemical characterization of the adsorbent. BET method was applied to measure the specific surface of BFS. The effect of various parameters, such as contact time, stirring speed, pH, temperature, particle size, and initial concentration, was examined to optimize the adsorption process. Adsorption isotherms were described by the Freundlich, Langmuir, Temkin, and Redlich-Peterson models. The adsorption kinetics was represented by the models of Lagergren and Blanchard. Also, the copper ions' transfer from the solution to the adsorbent was examined by determining the stages controlling the adsorption process. The thermodynamic study was undertaken to clarify the nature of the adsorption process as a function of temperature change.

Experimental

Blast furnace slag treatment

The samples of the considered slag were treated according to the process presented by Chouchane et al. [25]. This treatment was realized according to the following steps:

- Washing BF slag with distilled water;
- Air drying of samples for 48 hours;
- Grinding and sieving of samples to specific particle sizes, 200, 300, 400 and 500 μm ;
- Separation of samples by diameter size;
- Washing with distilled water and stoving at 105 $^{\circ}\text{C}$ of each batch;
- Storage in plastic boxes.

Analytic methods

The copper ions were determined by atomic absorption spectrometry (Perkin Elmer 3110). The pH of the solution was measured with a pH meter (Ericsson). The characterization of the solid samples was carried out by X-ray fluorescence (Siemens SRS 3000), and scanning electron microscope combined with energy dispersive analysis (Zeiss EVO MA25). The specific surface of the solid samples was measured using the Brunauer, Emmett and Teller model (BET model).

Experimental protocol

Several discontinuous mode tests were applied to study the nature of the copper adsorption phenomenon on the BF slag. The adsorption process was carried out by adding 1 g of prepared BFS to a 1 liter aqueous solution containing copper ions. Copper solutions were prepared from copper nitrate ($\text{Cu}(\text{NO}_3)_2 \cdot 3\text{H}_2\text{O}$) then dissolved in bidistilled water. Mixing of the solution was provided by a multi-speed stirrer. The temperature of the solution was controlled by a thermometer and adjusted using a water bath. The kinetics of copper elimination was determined by taking 5 ml samples every 20 minutes with a pipette, and these samples were filtered through filter paper. The kinetics of copper elimination were examined according to the protocol proposed by Chouchane et al. [25].

The determining parameters used in this adsorption process are the initial concentration (C_0 , mg/l), the agitation speed (V_{ag} , rpm), the hydrogen potential (pH), the temperature (T , $^{\circ}\text{C}$), and the particle size (\varnothing_s , μm). Moreover, the solution volume (V , L) is 1 liter and the solid mass (M , g) is 1 g throughout the study. The experimental conditions used are as follows:

- Equilibrium time, $C_0 = 30$ mg/L; $V_{ag} = 100$ rpm; pH = 4.7; $T = 20$ $^{\circ}\text{C}$; $\varnothing_s = 400$ μm ;

- Effect of agitation speed, $C_0 = 30$ mg/L; $V_{ag} = 50, 100, 150, 200$ rpm; $pH = 4.7$; $T = 20$ °C; $\varnothing_s = 400$ μm ;
 - Effect of initial pH, $C_0 = 30$ mg/L; $V_{ag} = 150$ rpm; $pH = 2, 3.9, 4.7, 5.2$; $T = 20$ °C; $\varnothing_s = 400$ μm ;
 - Effect of temperature, $C_0 = 30$ mg/L; $V_{ag} = 150$ rpm; $pH = 4$; $T = 20, 40, 50$ °C; $\varnothing_s = 400$ μm ;
 - Effect of particles size, $C_0 = 30$ mg/L; $V_{ag} = 150$ rpm; $pH = 4.7$; $T = 20$ °C; $\varnothing_s = 200, 300, 400, 500$ μm ;
 - Effect of initial concentration, $C_0, 10\text{--}100$ mg/L; $V_{ag} = 150$ rpm; $pH = 4.7$; $T = 20$ °C; $\varnothing_s = 300$ μm .
- The copper adsorption efficiency was calculated using Equation 1

$$\%R = \frac{C_0 - C_e}{C_0} \times 100, \quad (1)$$

where C_0 — the initial concentration solution (mg/L); C_e — the concentration of the solution at equilibrium (mg/L).

Desorption

The desorption process was performed using 10 g of the saturated BFS. The BFS collected by filter paper was washed, dried, and baked at 105 °C. Regeneration of saturated slag was accomplished using distilled water and different eluents, namely sulfuric acid (0.1N), nitric acid (0.1N), and hydrochloric acid (0.1N). Desorption was performed with stirring (100rpm) at room temperature. The efficiency of the desorption process was evaluated using Equation 2:

$$\text{Desorption rate} = \frac{q_{des}}{q_{ads}} \times 100, \quad (2)$$

where q_{ads} — the adsorbed quantity at equilibrium (mg/g) for cycle I; q_{ads} — the desorbed quantity at equilibrium (mg/g) of each cycle.

The experimental protocol for copper desorption from saturated BFS was applied according to the approach carried out by Chouchane et al. [25].

Results and Discussion

Characterization of BF slag

According to our previous work [25] and subsequent recent analyses, BFS consists of silica (37.16 %), lime (40.11 %), alumina (14.34 %), magnesium oxide (5.34 %), and a low percentage of oxides. Indeed, the results of the analyses carried out by XRF, XRD, and SEM-XDE specified that BFS consists mainly of SiO_2 , CaO , Al_2O_3 , and MgO . These studies also revealed the presence of a small amount of oxides, namely Fe_2O_3 , MnO , K_2O , and Na_2O , as shown in Table 1 and Figures 1 and 2. BFS grains were found to be conchoidal in shape, with a wide grain size distribution, smooth surfaces of the grain edges visible, and no visible porous structure in the images shown in Figure 3. According to the research results the specific surface was shown to be $238 \text{ m}^2 \cdot \text{g}^{-1}$.

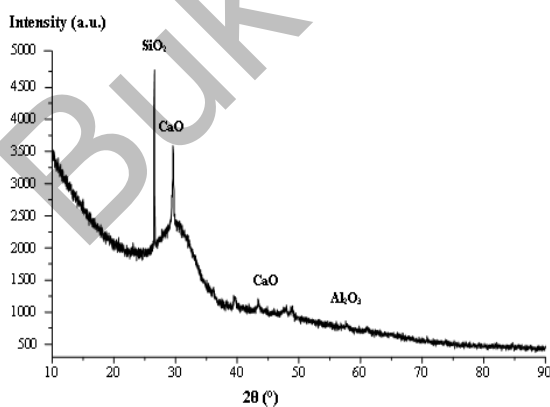


Figure 1. Diffractogram of BFS sample [25]

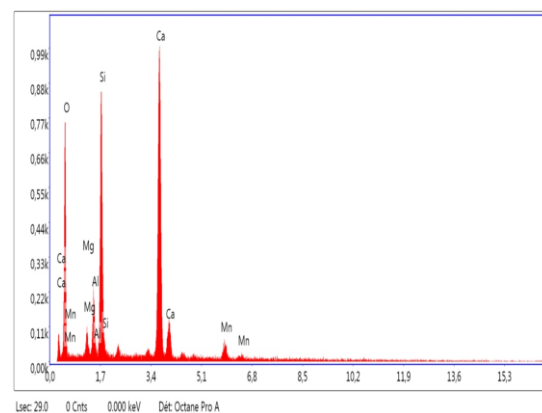


Figure 2. EDX results

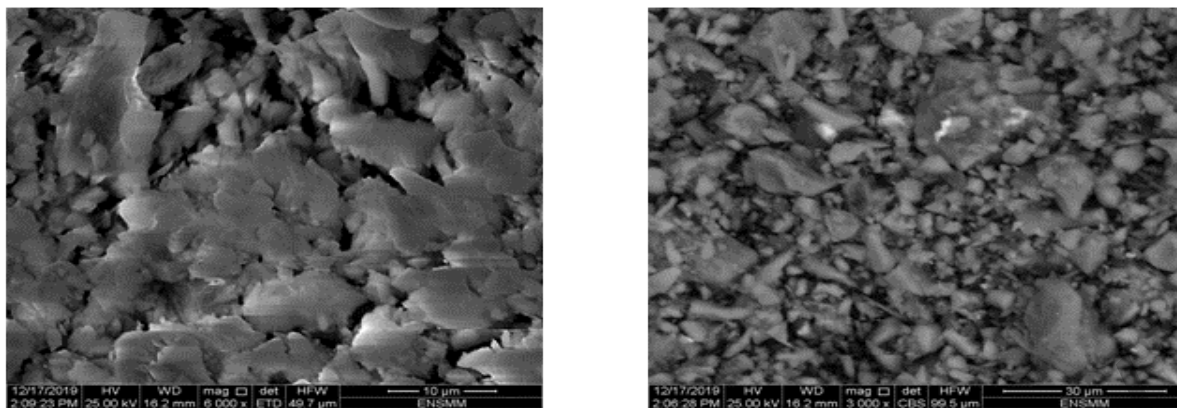


Figure 3. SEM images of BFS

Contact time effect

In the adsorption process, the contact time effect is a determining factor because it informs us about the equilibrium time and the stages of pollutant removal. The kinetic study of the copper adsorption on BFS showed that equilibrium is reached after 140 minutes of stirring under specific experimental conditions (Fig. 4). Indeed, the adsorbed amount becomes constant ($C_e/C_0 = \text{constant}$) after 140 minutes of stirring. This effect is regenerated due to the progressive reduction of active adsorption sites until total saturation of the adsorbent [26]. This finding prompted us to take 140 min as equilibrium contact time.

Table 1

Composition of blast furnace slag (BFS) [25]

Substance	% mass
CaO	40.11
Al ₂ O ₃	14.34
SiO ₂	37.16
MgO	5.34
Fe ₂ O ₃	1.91
MnO	0.69
K ₂ O	0.28
Na ₂ O	0.37

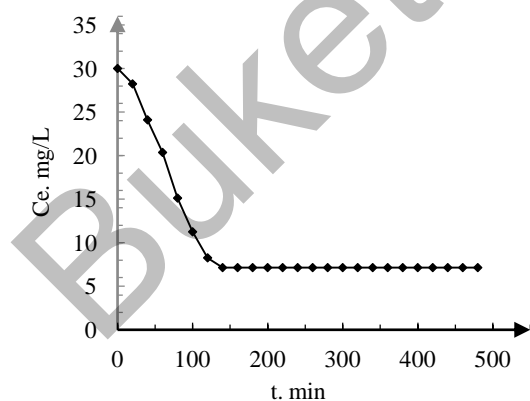


Figure 4. Contact time effect

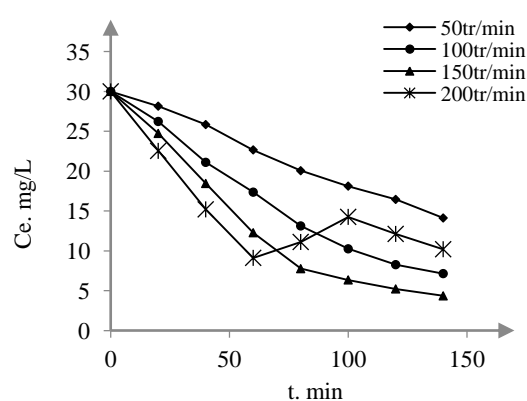


Figure 5. Effect of agitation speed

Agitation speed effect

Agitation of the solution is an extremely decisive operation in adsorption processes. In fact, it favors the diffusion of the adsorbate toward the solid [27, 28]. Stirring speeds utilized were 50, 100, 150, and 200 rpm, respectively (Fig. 5).

Figure 5 shows that the amount of copper adsorbed by BFS gradually increased with increasing stirring speed until it reached 150 rpm. However, fluctuations in the value of the residual concentration after 80 minutes of agitation were noticed at 200 rpm. These fluctuations are probably caused by copper desorption from the BFS after strong agitation [29]. Based on this outcome, we conclude that the solution stirring contributed effectively to the diffusion of copper ions from the solution into the adsorbent, which gives it an important role in external diffusion [30]. In addition, we identified 150 rpm as the optimal agitation speed.

Effect of initial solution pH

The pH of the medium is a significant element in this process, since it affects both the shape of the ions and the surface of the adsorbent [31]. Several media were used during these experimental tests, namely pH 2, pH 3.9, pH 4.7, and pH 5.2 (Fig. 6).

Experimental data showed that Cu(II) adsorption is unfavourable at pH 2 (Fig. 6). This phenomenon is explained by the presence of H^+ protons, which obstruct the adequate transfer of Cu(II) ions from the solution to the adsorbent [32]. Moreover, a change in pH from 2 to 4.7 had a positive effect on the adsorption process [33], where we observed that the residual concentration at equilibrium decreased from 19.87 mg/L to 4.35 and the removal rate increased from 33.7 % to 85.5 %.

For solutions at pH 5.2, the values of the capacity and adsorption rate are less important and regressed from 25.67 to 18.11 mg/g and from 85.5 to 60.36 % respectively. This result could be explained by the fact that precipitation dominates the removal of the copper and adsorption has an almost negligible effect [34]. It is important to note that the pH threshold for Cu^{2+} speciation into hydroxides is approximately 5.0–5.5 [35].

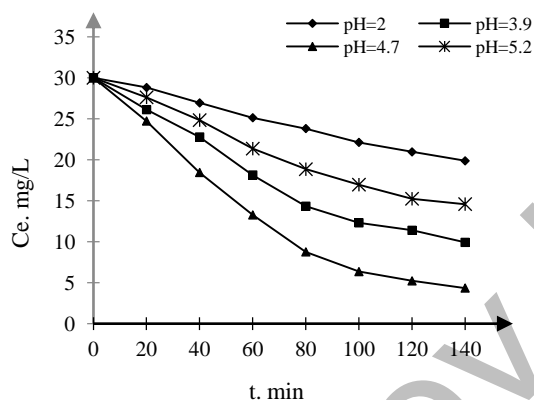


Figure 6. Effect of initial pH

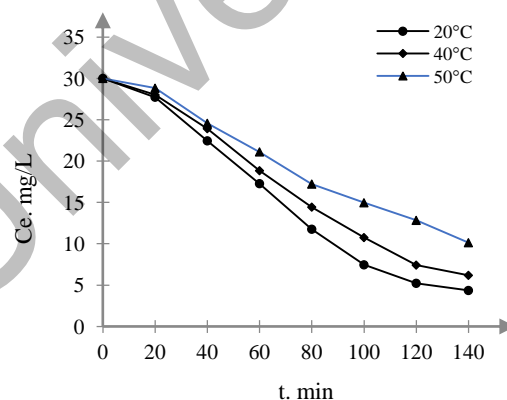


Figure 7. Effect of temperature

Effect of Temperature

The temperature of the solution is an important characteristic in the adsorption process, since it makes a huge contribution to the fixation of metals on the surface of a solid [36]. For this purpose, the effect of temperature on the Cu(II) adsorption process on BFS was studied (Fig. 7).

The experimental data revealed that the temperature has an inversely proportional effect on the Cu(II) adsorption process and this phenomenon is more favorable at 20 °C (Fig. 7). This result allowed us to predict that the copper adsorption on BFS in solution is exothermic [37]. The inefficiency of the copper adsorption process as temperature rises is most likely due to the destruction of active binding adsorption sites [38] or the reduction in attractive Cu(II)/BFS bonds [39]. Furthermore, evaporation of the solution can occur at high temperatures, which affects the concentration of Cu(II) ions in the solution.

Effect of the granulometry of the solid

The granulometry of the adsorbent has a significant effect on the rate of ion transfer from the adsorbate to the solid [40]. In this perspective, we proceeded to evaluate the effect of particle size on copper adsorption using different diameters, namely 200, 300, 400, and 500 μm (Fig. 8).

From the kinetic study, it was observed that copper adsorption is better for particles with sizes corresponding to 300 μm and begins to weaken with increasing particle size. Indeed, the adsorption yield decreased from 91.73 % to 85.5 % and then to 70.5 % as the size of the particles widened. An increase in particle size led to a narrowing of the specific surface area, which in turn led to a decrease in the adsorption capacity of the solid [41, 42]. The experimental results also showed that the copper adsorption on the BFS with

a diameter of 200 μm is estimated as unfavourable (Fig. 8). This repercussion could probably be clarified by the appearance of the coalescence phenomenon [43].

Effect of the initial solution concentration

The elimination of copper on BFS under the effect of the initial concentration [10-100 mg/L] was studied under our experimental conditions, namely $V_{ag} = 150$ rpm; pH = 4.7; $\emptyset = 300$ μm , $T = 20$ $^{\circ}\text{C}$. Maximum adsorption capacity at equilibrium was calculated using Equation 3:

$$q_e = \frac{C_0 - C_e}{m} \times V, \quad (3)$$

where C_0 — the initial solution concentration (mg/L); C_e — the solution concentration at equilibrium (mg/L); m — the adsorbent mass (1 g); V — the solution volume ($V = 1$ L).

The dependence of the adsorbed capacity (q_e) on the initial concentration (C_0) is shown in Figure 9. As can be seen in Figure 9, the adsorbed amount increased in proportion the initial concentration up to a certain amount ($C_0 = 80$ mg/L), after which the adsorbed amount remained constant. Indeed, with an increase in the concentration of the initial solution, the probability of BFS/Cu(II) contact rises, which contributes to an increase in the adsorbed amount. But once the adsorption sites are saturated, the increase in the initial concentration could not affect the adsorption process [44, 45]. The amount adsorbed (q_e) at the saturation level is 45.16 mg/g, which represents the maximum capacity adsorbed by 1 g of BFS.

Based on these results, we concluded that the sorption rate is controlled by the initial concentration, which varies from 10 to 80 mg/L. On the other hand, the maximum amount adsorbed per gram of BFS is 45.16 mg/g.

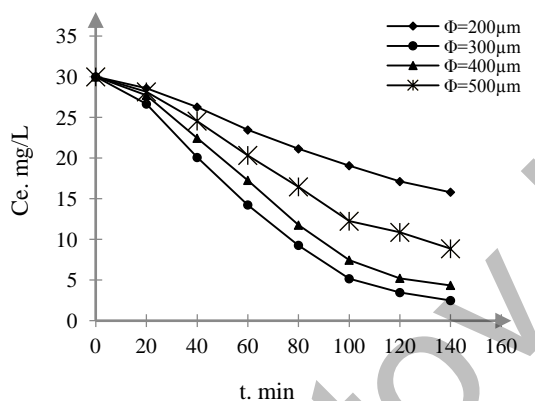


Figure 8. Effect of the granulometry of the solid

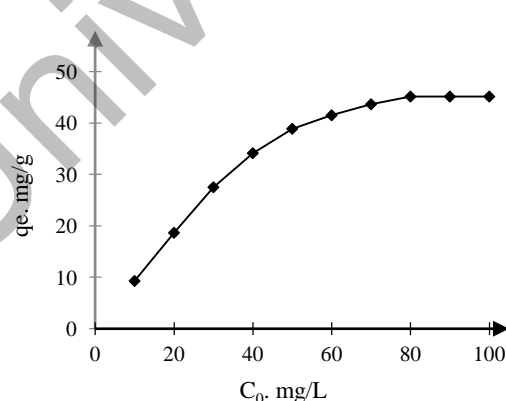


Figure 9. Effect of initial concentration

Adsorption isotherms

In order to study the correlation between adsorbent and adsorbate and determine the best adopted presentation for the experimental data, we applied the adequate adsorption isotherms, namely Freundlich [46], Langmuir [47], Temkin [48] and Redlich-Peterson [49]. Their empirical formulas are given by Equations 4-7, respectively.

$$\ln q_e = \ln k + \frac{1}{n} \ln C_e; \quad (4)$$

$$\frac{C_e}{q_e} = \frac{1}{q_{max}} C_e + \frac{1}{q_{max} b}; \quad (5)$$

$$q_e = B_T \ln A_T + B_T \ln C_e; \quad (6)$$

$$\ln \frac{C_e}{q_e} = g \ln C_e - \ln k_R, \quad (7)$$

where q_e — the adsorbed capacity at equilibrium (mg/g); C_e — the concentration of solution at equilibrium (mg/L); q_{max} — the maximum adsorbed capacity (mg/g); b — the thermodynamic constant of the adsorption equilibrium ($\text{L} \cdot \text{mg}^{-1}$); k_F and $1/n$ — the Freundlich constants related to adsorption and affinity; A_T — Temkin isotherm equilibrium binding constant (L/g); b_T — Temkin isotherm constant; R — the universal gas

constant ($8.314 \text{ J/K}\cdot\text{mol}$); T — the temperature (298K); B_T — the constant related to heat of sorption ($\text{KJ}\cdot\text{kmol}^{-1}$); k_R — the intercept (L/g); g — the Redlich-Peterson isotherm constants.

The parameter values of the Freundlich, Langmuir, Temkin, and Redlich-Peterson models are grouped in Table 2. The presentations of these models are sequentially shown in Figures 10 to 13.

As can be seen from the data presented in Table 2, the Langmuir's model is best suited for this process. Indeed, the correlation coefficient of the Langmuir model ($R^2=0.99$) is higher than those of all other considered models. Moreover, the adsorbed capacity measured from the Langmuir model was closest to the experimental adsorption value.

Based on these results, it was confirmed that the adsorption process takes place on a homogeneous monolayer surface. This leads us to specify that all active sites of adsorption have similar interactions with copper [47].

Figure 14 shows that the adsorption isotherm is L-type, undergoes a fast phase in the low concentration range, is followed by a medium-weak phase, and ends with a phase constant (the appearance of a long horizontal plateau). This identification provides information about the formation of a monolayer [6, 26]. In the same context, Chouchane et al. [25] reported that the adsorption of nickel on the blast furnace slag was accomplished on a homogeneous monolayer. Zahar, M.M.S., Muhammad, S.N. et al. also stated in [50] that the manganese sorption in solution on steel slag occurred on a homogeneous monolayer layer.

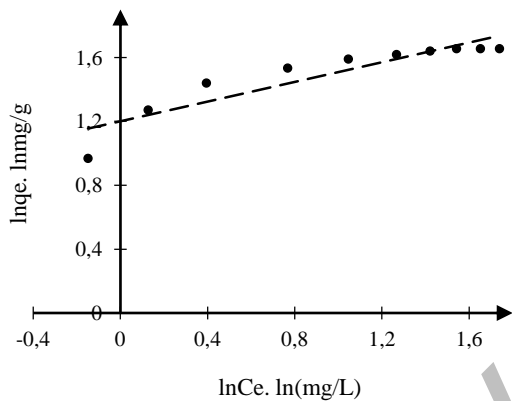


Figure 10. Presentation of the Freundlich model

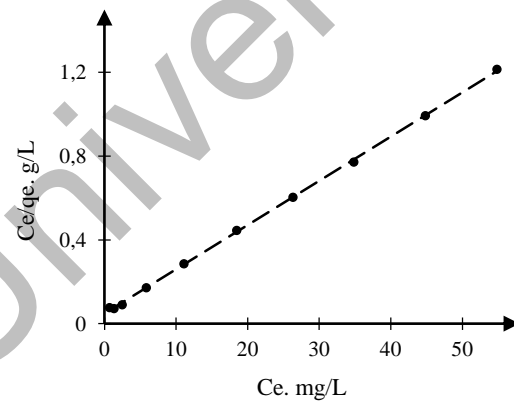


Figure 11. Presentation of the Langmuir model

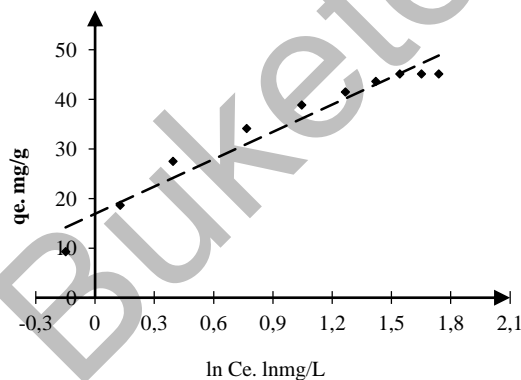


Figure 12. Presentation of the Temkin model

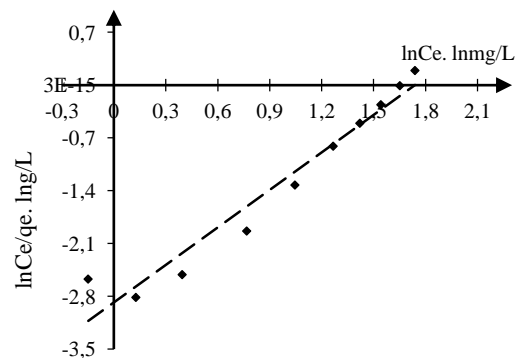


Figure 13. Presentation of the Redlich-Peterson model

According to the value of the Temkin model parameter ($b_t = 0.261$), we conclude that the adsorption of copper on BFS in solution is physical [25]. On the other hand, the parameter values of the Freundlich ($n = 3.7$) and Redlich-Peterson ($g = 0.68$) models confirm that this adsorption process is favorable [1, 20, 44, 49].

The quality of the adsorption process can also be defined by the Equilibrium parameter of Langmuir equation R_L . The R_L qualifies the adsorption process as favorable if it is between 0–1 ($0 < R_L < 1$), unfavora-

ble if it is greater than 1 ($R_L > 1$) and linear if it is equal to 1 ($R_L = 1$) [51]. This ratio was calculated as follows (Equation 8):

$$R_L = \frac{1}{1 + C_0 b}, \quad (8)$$

where R_L — the Ratio indicates the quality of the adsorption; B — the Langmuir isotherm constant; C_0 — the initial solution concentration.

As can be seen from Figure 15, the R_L value decreases from 0.18 to 0.02 as C_0 increases. This result also confirmed the favorable nature of copper adsorption by BFS.

Table 2

Isotherm parameters for adsorption of copper by BF slag

Models	Parameters			
Freundlich	$q_{e_{exp}}$, mg/g	K_F , $(\text{mg} \cdot \text{g}^{-1})(\text{ml} \cdot \text{mg}^{-1})^{1/n}$	n	R^2
	45.16	0.183	3.25	0.836
Langmuir	$q_{e_{exp}}$, mg/g	q_{max} , mg/g	B , $\text{L} \cdot \text{mg}^{-1}$	R^2
	45.16	46.31	0.437	0.997
Temkin	$q_{e_{exp}}$, mg/g	A_T , L/g	b_T , $\text{KJ} \cdot \text{mol}^{-1}$	R^2
	45.16	1.06	0.214	0.944
Redlich-Peterson	$q_{e_{exp}}$, mg/g	g	k_R , L/g	R^2
	45.16	0.651	17.77	0.993

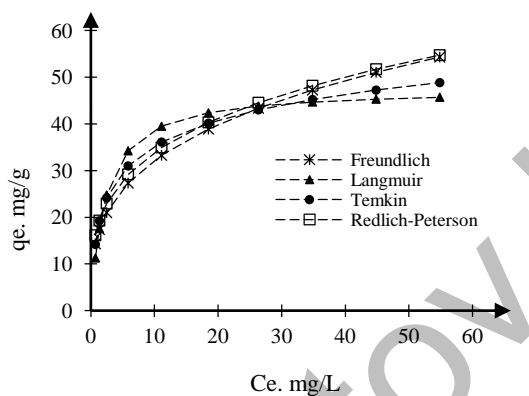


Figure 14. Presentation of the Freundlich model

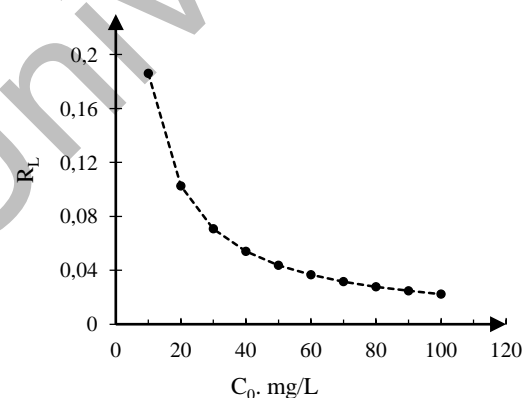


Figure 15. Presentation of the Langmuir model

Adsorption Kinetics

The kinetic study is a significant step in the solid-liquid adsorption process because it facilitates the understanding of the adsorption rate and the behavior of the adsorbents compared to the adsorbates at time t and at equilibrium [52]. The pseudo first and pseudo-second orders were determined under optimal conditions by the frequently used kinetic models, namely the Lagergren and Blanchard models, respectively.

The Lagergren relationship [53] was formulated to illustrate sorption kinetics in a liquid-solid environment. Its relation is represented by Equation 9:

$$\log(q_e - q) = -k_L t + \log q_e \quad (9)$$

Blanchard's model [54] was formulated to describe the pseudo-second order of the adsorption process. It is represented by Equation 10:

$$\frac{t}{q} = \frac{1}{k_b q_e^2} + \frac{t}{q_e} \quad (10)$$

where q_e — the adsorbed capacity at equilibrium (mg/g); q — the adsorbed capacity at time t (mg/g); k_L — the constant of Lagergren model (min^{-1}); k_b — the constant of Blanchard model ($\text{g}/\text{mg} \cdot \text{min}$); t — the time of adsorption process (min).

The parameters of the Lagergren and Blanchard models are represented in Table 3. These two models are shown graphically in Figures 16 and 17.

From the literature, the Lagergren and Blanchard models are satisfied (if the R^2 correlation coefficients are greater than 0.9, and the experimental and calculated adsorption capacities are close [34, 35, 55, 56]).

As can be seen in Table 3, the correlation coefficient of the Blanchard model (0.988) is higher than that of the Lagergren model (0.912), and the experimental adsorption capacity (45.16 mg/g) was close to that calculated per the Blanchard equation (45.88 mg/g). This result indicates the existence of a proportionality between the adsorption active sites and the adsorbed copper ions, which is compatible with the pseudo-second-order model. The pseudo-first-order model with the lowest regression ($R^2 = 0.912$) indicates that adsorption can occur on a monolayer surface, which reaffirms our previous results, namely that the Langmuir model is best suited to the process of copper adsorption on slag [57].

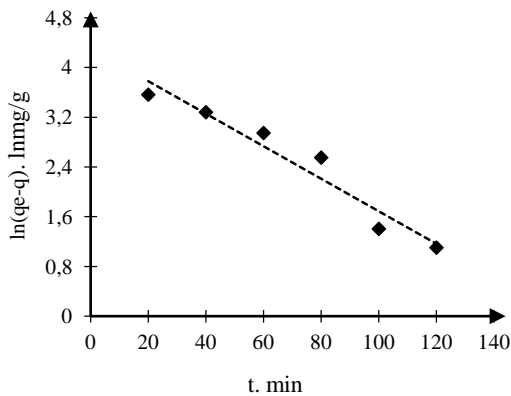


Figure 16 Pseudo-first order kinetic

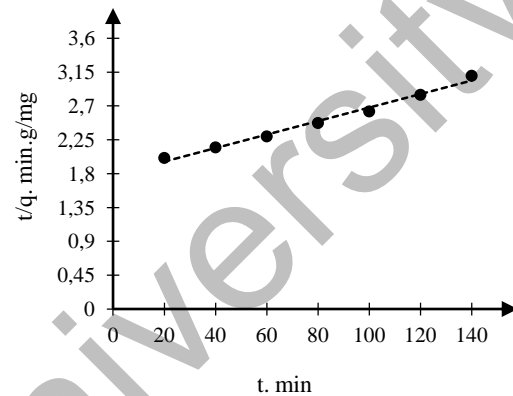


Figure 17 Pseudo-second order kinetic

Based on these results, it was concluded that the Blanchard model is best suited to describe the kinetics of copper adsorption on BFS. In the same context, Xue et al. [34] reported that copper removal from basic oxygen furnace slag follows pseudo-second order kinetics. Chouchane et al. [25] also indicated that the adsorption of nickel on the slag at different temperatures follows the kinetics of the pseudo-second order.

In order to study the mechanism of the transfer of copper ions from the solution to the surface of the BFS, we tried to identify the limiting stages of this phenomenon, namely the external and the Intraparticle diffusion.

External diffusion is represented by Equation 11 [58]:

$$\ln C_e = k_{ext} t + C_{ext} \quad (11)$$

where C_e — the concentration of solution at equilibrium (mg/L); t — the time measured in minute; k_{ext} — the diffusion constant (min^{-1}); C_{ext} — the intercept ($\ln(\text{mg/L})$).

According to the bibliography, copper adsorption is controlled by external diffusion if the plot of the function $\ln C_e = f(t)$ is linear and also if the correlation coefficient is greater than 0.9 [35, 59]. As can be seen from Table 5 and Figure 18, the plot is linear and the correlation coefficient exceeds 90 % ($R^2 = 0.99$). This result shows that the adsorption of copper by the blast furnace slag is controlled by external diffusion.

The Weber-Morris model equation (internal diffusion) is represented below (Equation 12) [60]:

$$q = k_w (t)^{1/2} + C_{int} \quad (12)$$

where q — the quantity adsorbed at time t (mg/g); t — the time measured in minute; k_w — the diffusion rate constant in the pores ($\text{mg/m} \cdot \text{min}^{1/2}$); C_{int} — the intercept and it's tied to the boundary layer.

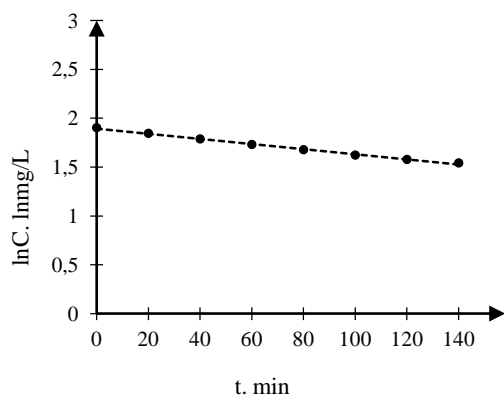


Figure 18. External diffusion kinetic

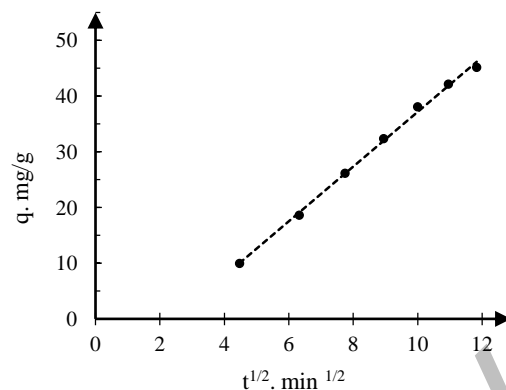


Figure 19. Intra-particle diffusion kinetic

The parameters of Weber-Morris model are presented in Table 3 and the graphic representation is illustrated in Figure 19. It is known from previous studies that the adsorption process is controlled by internal diffusion if the plot of the function $q_e = f(t^{1/2})$ is linear and passes through the origin [1, 26, 61].

As can be seen in Figure 19, the plot of the function $q_e = f(t^{1/2})$ is multilinear, but does not pass through the origin ($C \neq 0$), which means that internal diffusion is not the only mechanism controlling copper adsorption kinetics. Furthermore, multi-linearity argues for the existence of various mechanisms controlling the adsorption process, which reaffirms our inference that copper adsorption by BFS is controlled by both external and internal diffusion [25, 62, 63].

Table 3

Kinetic model parameters

Models	Parameters			
Lagergren	$q_{e_{exp}}$, mg/g	K_{lag} , min^{-1}	$q_{e_{theo}}$, mg/g	R^2
	45.16	2.9×10^{-2}	50.58	0.912
Blanchard	$q_{e_{exp}}$, mg/g	K_b , g/mg min	$q_{e_{theo}}$, mg/g	R^2
	45.16	1.8×10^{-3}	45.88	0.988
Internal diffusion	$q_{e_{exp}}$, mg/g	C_{int}	k_w , mg/g.min	R^2
	45.16	11.97	4.31	0.995
Internal diffusion	$q_{e_{exp}}$, mg/g	C_{ext}	K , min^{-1}	R^2
	45.16	1.86	0.02	0.998

Thermodynamic study

Under the effect of the temperature of the solution and the conditions of the experiment, a thermodynamic study was carried out to give a more detail about the character of the copper adsorption process. Parameters such as free enthalpy variation (ΔG^0), enthalpy change (ΔH^0) and entropy change (ΔS^0) were determined to define the nature of the adsorption process. These variables were determined from the following equations (Equations 13–15):

$$\Delta G^0 = -RT \ln k_d ; \quad (13)$$

$$\Delta G^0 = \Delta H^0 - T \Delta S^0 ; \quad (14)$$

$$\ln k_d = \frac{\Delta H^0}{R} \times \frac{1}{T} + \frac{\Delta S^0}{R} . \quad (15)$$

The distribution coefficient k_d was calculated from the ratio of the adsorbed quantity to the residual concentration at equilibrium [59, 64]:

$$k_d = \frac{C_i - C_e}{C_e} \times \frac{V}{M} = \frac{q_e}{C_e} , \quad (16)$$

where q_e — the adsorbed quantity at equilibrium (mg/g); C_i — the initial concentration of solution (mg/L); C_e — the residual concentration at equilibrium (mg/L); T — the absolute temperature (K); R — the universal gas constant; k_d — the distribution coefficient (L/g); V — the volume of solution (1 L); M — the mass of the adsorbent (1 g).

The plot of the function $\ln k_d = f\left(\frac{1}{T}\right)$ at different temperatures is presented in Figure 20. The thermodynamic parameter values are grouped in Table 4.

Initially, it was observed that the adsorption efficiency was inversely proportional to the temperature, as presented in Figure 7. This result led us to predict that the nature of the adsorption process is exothermic. Following the thermodynamic study, this prediction was verified by the negative value of ΔH^0 displayed in Table 3 [20, 25, 65].

Table 4 also shows that the values of ΔG^0 and ΔS^0 are negative. Negative values of ΔG^0 inform us about the spontaneity and feasibility of the adsorption process [6, 66, 67]. Furthermore, the negative value of ΔS^0 informs us about the decrease in the randomness of copper adsorption at the solid/solution interface [6, 57, 68]. Indeed, this weakening in randomness is probably due to the structural stability of BFS during the adsorption process.

It was also observed from Table 4 that the absolute value of the Gibbs free energy increased with increasing temperature. This effect indicates that higher temperatures help to increase the driving force of adsorption [69]. It was found from Figure 20 that the distribution coefficient k_d decreases with increasing temperature. This result points out that the high-temperature adsorption process is less efficient [59].

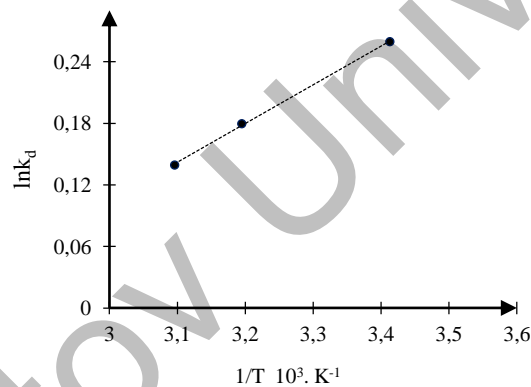


Figure 20. Van't Hoff plot for copper adsorption

Table 4

Thermodynamic parameters of the copper adsorption on BFS

T, K	$\Delta G^0, kJ/mol$	$\Delta H^0, kJ/mol$	$\Delta S^0, J/mol \cdot K$
293	-17.45	-3.13	-8.54
313	-18.42		
323	-18.92		

Desorption study

The desorption of the copper ions from the charged BFS is a very important process since it allows us to reuse the same adsorbent and avoids the storage of another type of pollution [1, 3]. For this study, we performed desorption of the Cu(II) adsorbed on the loaded BFS in various solutions.

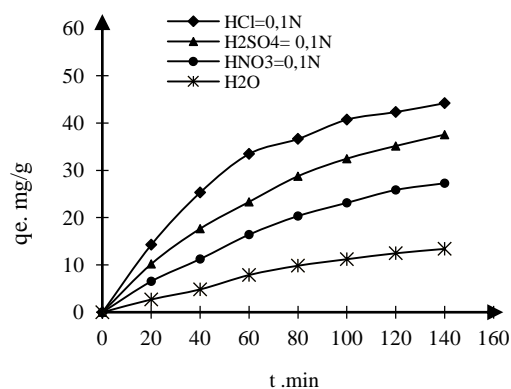


Figure 21. Desorption kinetics

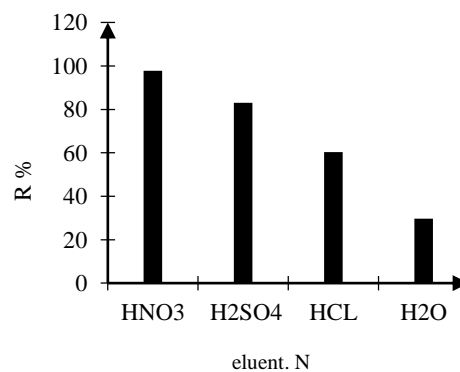


Figure 22. Desorption rate (%)

The kinetics of Cu(II) desorption, as well as the effects of the solutions used, are depicted in Figures 21 and 22. Table 5 shows the results of the various cycles used (adsorption and desorption).

Table 5

Adsorption and desorption performance of copper

	$q_{e_{ads}}$, mg/g	$q_{e_{des}}$, mg/g	Desorption rate, %
Cycle I	45.16	44.19	97.85
Cycle III	42.64	39.93	93.64
Cycle V	38.36	35.11	91.52
Cycle VI	32.18	22.27	69.2
Cycle VII	20.14	7.15	35.5

The results of the experiments revealed that desorption of Cu(II) from the surface of saturated BFS is more efficient with 0.1N HCl. Indeed, as can be seen in Figure 22, the desorption rates were 98.91 %, 84.19 %, 70.64 %, and 27.34 % in the presence of HCl, H₂SO₄, HNO₃, and H₂O respectively. Consequently, hydrochloric acid (HCl, 0.1 N) was retained as the regeneration eluent.

Based on the data in Table 5, it was found that the blast furnace slag as an adsorbent could be exploited over three consecutive cycles where the adsorption rate is greater than 91 %. However, a glaring regression was displayed for the last two cycles. This alteration is certainly caused by the loss of mass and/or the deterioration of the surface of the adsorbent used [26, 58, 69].

Conclusions

In general, based on the results of the study, it can be concluded that the adsorption of copper on the blast furnace slag is feasible and favorable with a yield of 91.7 %. The physicochemical analysis indicated that blast furnace slag mainly consists of lime, silica, alumina, and magnesium oxide, with a moderately high specific surface (238 m²/g). Experimental data showed that the maximum adsorption capacity is 45.16 mg/g after 140 minutes under the optimal conditions, namely: $V_{ag} = 150$ rpm; pH = 4,7; $\varnothing_s = 300$ μ m, $T = 20$ °C, $M_s = 1$ g. Modeling of the experimental data revealed that the copper adsorption process is more consistent with Langmuir's model ($R^2 = 0.99$). Adsorption is best described by the pseudo-second order kinetics model, with a correlation coefficient of 0.99. The adsorption mechanism was studied, and it was discovered that the adsorption process is physical, with copper diffusion from solution toward the adsorbent controlled by external and internal diffusion in sequential order. The thermodynamic study demonstrated that the adsorption process is feasible, exothermic, spontaneous, and has less entropy. The executed desorption process indicated that the BFS can be effectively regenerated over three consecutive cycles in the presence of hydrochloric acid (HCl, 0.1 N) as an eluent. Based on the data obtained, it can be concluded that adsorption on the BFS will be an effective outcome in toxic metal elimination processes.

Acknowledgments

The authors declare that they have no known competing financial interests or personal relationships that could have appeared to influence the work reported in this paper. They deeply thank the staff of the chemistry laboratory (Unit of Applied Steel Research, URASM/CRTI Annaba, Algeria) for their help.

References

- 1 Çelebi, M. & Gökirmak Söğüt, E. (2022). High-efficiency removal of cationic dye and heavy metal ions from aqueous solution using amino-functionalized graphene oxide, adsorption isotherms, kinetics studies, and mechanism. *Turkish Journal of Chemistry*, 46, 1577–1593. <https://doi.org/10.55730/1300-0527.3462>
- 2 Yan, X., Wang, J., Zhu, L., Wang, J., Li, S. & Kim, M. (2021). Oxidative stress, growth inhibition, and DNA damage in earthworms induced by the combined pollution of typical neonicotinoid insecticides and heavy metals. *Science of the Total Environment*, 754. <https://doi.org/10.1016/j.scitotenv.2020.141873>.
- 3 Asliyüce Çoban, S., Safarik, I. & Denizli, A. (2021). Heavy metal removal with magnetic coffee grain. *Turkish Journal of Chemistry*, 45, 157–166. <https://doi.org/10.3906/kim-2006-47>
- 4 Amin, A., Shima, S., Hafez, W. & Desouky, O. (2021). Biorecovery of Copper (II) using *Klebsiella pneumoniae* Isolated from Wastewater Effluents. *Egyptian Journal of Chemistry*, 64, 6623–6633. <https://doi.org/10.21608/EJCHEM.2021.78714.3847>
- 5 Ayandiran, T.A., Fawole, O.O. & Dahunsi, S.O. (2018). Water quality assessment of bitumen polluted Oluwa River. South-Western Nigeria. *Water Resources and Industry*, 19, 13–24. <https://doi.org/10.1016/j.wri.2017.12.002>
- 6 Tunçeli, A., Ulaş, A., Acar, O. & Türker, A.R. (2022). Adsorption isotherms, kinetic and thermodynamic studies on cadmium and lead ions from water solutions using Amberlyst 15 resin. *Turkish Journal of Chemistry*, 46, 193–205. <https://doi.org/10.3906/kim-2107-28>
- 7 Kanagaraj, P., Nagendran, A., Rana, D., Matsuura, T., Neelakandan, S., Karthikkumar, T. & Muthumeenal, A. (2015). Influence of N-phthaloyl chitosan on poly (etherimide) ultrafiltration membranes and its application in biomolecules and toxic heavy metal ion separation and their antifouling properties. *Applied Surface Science*, 329, 165–173. <https://doi.org/10.1016/j.apsusc.2014.12.082>
- 8 Luo, J.M., Tao, X.Y., Zhang, J., Xia, Y., Huang, H., Zhang, L.Y., Gan, Y.P., Liang, C. & Zhang, W.K. (2016). Sn⁴⁺ ion decorated highly conductive Ti₃C₂MXene, promising lithium-ion anodes with enhanced volumetric capacity and cyclic performance. *ACS Nano*, 10, 2491–2499. <https://doi.org/10.1021/acsnano.5b07333>
- 9 Dabrowski, A., Hubicki, Z., Podkoscielny, P. & Robens, E. (2004). Selective Removal of the Heavy Metal Ions from Waters and Wastewaters by Ion-exchange Method. *Chemosphere*, 56(2), 91–106. <https://doi.org/10.1016/j.chemosphere.2004.03.006>
- 10 Ma, H.F., Yang, J., Gao, X., Liu, Z., Liu, X. & Xu, Z. G. (2019). Removal of chromium (VI) from water by porous carbon derived from corn straw, influencing factors, regeneration and mechanism. *Journal of Hazardous Materials*, 369, 550–560. <https://doi.org/10.1016/j.jhazmat.2019.02.063>
- 11 Kaprara, E., Tziarou, N., Kalaitzidou, K., Simeonidis, K., Balcells, L., Pannunzio, E.V., Zouboulis, A. & Mitrakas, M. (2017). The use of Sn(II) oxy-hydroxides for the effective removal of Cr(VI) from water, optimization of synthesis parameters. *Science of The Total Environment*, 605–606, 190–198. <https://doi.org/10.1016/j.scitotenv.2017.06.199>
- 12 Guerra, E.R., Aristizabal, J., Arce, B., Zurob, E., Dennett, G., Fuentes, Ro., Suescún, A.V., Cardenas, L., Rodrigues da Cunha, T.H., Cabezas, R., García-Herrera, C. & Parra, H.C. (2021). Nanostructured Didymospheniageminata-based membrane for efficient lead adsorption from aqueous solution. *Journal of Environmental Chemical Engineering*, 9(4), 105269. <https://doi.org/10.1016/j.jece.2021.105269>
- 13 Yusuf, M., Chuah, L., Khan, M.A. & Choong, T.S. (2014). Adsorption of Nickel on Electric Arc Furnace Slag, Batch and Column Studies. *Separation Science and Technology*, 49(3), 388–397. <https://doi.org/10.1016/j.jece.2021.105269>
- 14 Zhou, H., Ai J., Gao, H., Zhang, W. & Wang, D. (2020). Removal of arsenic in groundwater using Slag based calcined layered double hydroxides (CLDHs) with dual functions of adsorption and photo-catalysis. *Colloids and Surfaces A. Physicochemical and Engineering Aspects*, 604, 125300. <https://doi.org/10.1016/j.colsurfa.2020.125300>
- 15 El-Dars, F.M.S.E., Elngar, M.A.G., Abdel-Rahim, S.Th, El-Hussiny, N.A. & Shalabi M.E.H. (2015). Kinetic of nickel (II) removal from aqueous solution using different particle size of water-cooled blast furnace slag. *Desalination and Water Treatment*, 54, 769–778. <https://doi.org/10.1080/19443994.2014.904071>
- 16 Vu, M.T., Nguyen, L.N, Johir, M.A.H, Ngo, H.H., Skidmore, C. Fontana, A., Galway, B., Bustamante, H. & Nghiem, L. D. (2020). Phosphorus removal from aqueous solution by steel making slag — Mechanisms and performance optimization. *Journal of Cleaner Production*, 284, <https://doi.org/10.1016/j.colsurfa.2020.125300>
- 17 Scott, I.S.P.C. & Penn, J.C. (2021). Estimating the variability of steel slag properties and their influence in phosphorus removal ability. *Chemosphere*, 276, 130205. <https://doi.org/10.1016/j.chemosphere.2021.130205>
- 18 Xue, Y., Hou, H. & Zhu, S. (2009). Adsorption removal of reactive dyes from aqueous solution by modified basic oxygen furnace slag, Isotherm and kinetic study. *Chemical Engineering Journal*, 147, 272–279. <https://doi.org/10.1016/j.cej.2008.07.017>
- 19 Dhmees, AS., Khaleel, N. M. & Mahmoud, S.A. (2018). Synthesis of silica nanoparticles from blast furnace slag as cost-effective adsorbent for efficient azo-dye removal. *Egyptian Journal of Petroleum*, 27(4), 1113–1121. <https://doi.org/10.1016/j.ejpe.2018.03.012>

- 20 Donat, R. (2022). Removal of Cd^{2+} metal ions from aqueous solutions by Na-alginate-containing composite biosorbent. *Turkish Journal of Chemistry*, 46, 754–765. <https://doi.10.55730/1300-0527.3365>
- 21 Shotop, M.Y. & Al-Suwiti, I.N. (2021). The possible role of vitamins E and C in reducing the toxicity of copper nanoparticles in the kidney and liver of the rats (*Rattus norvegicus*). *Journal of King Saud University-Science*, 33(2), 101357. <https://doi.10.1016/j.jksus.2021.101357>
- 22 Tauetsile, P.J., Oraby, E.A. & Eksteen, J.J. (2018). Adsorption behaviour of copper and gold Glycinates in alkaline media onto activated carbon. Part 2, Kinetics. *Hydrometallurgy*, 178, 195–201. <https://doi.10.1016/j.hydromet.2018.04.016>
- 23 Ben Ali, M., Wang, F., Boukherroub, R., Lei, W. & Xia, M. (2019). Phytic acid-doped polyanilinenanofibers-clay mineral for efficient adsorption of copper (II) ions. *Journal of Colloid and Interface Science*, 553, 688–698. <https://doi.10.1016/j.jcis.2019.06.065>
- 24 Bashir, M., Tyagi, S. & Annachhatre, A.P. (2020). Adsorption of copper from aqueous solution onto agricultural Adsorbents, Kinetics and isotherm studies. *Materials Today, Proceedings* 28, 1833–1840. <https://doi.10.1016/j.jcis.2019.06.065>
- 25 Chouchane, T., Khireddine, O. & Boukari, A. (2021). Kinetic studies of Ni(II) ions adsorption from aqueous solutions using the blast furnace slag (BF slag). *Journal of Engineering and Applied Science*, 68, 34. <https://doi.10.1186/s44147-021-00039-3>
- 26 Chouchane, T. & Boukari, A. (2022). Impact of influencing parameters on the adsorption of nickel by kaolin in an aqueous medium, *Analytical and Bioanalytical Chemistry Research*, 9(4), 381–399. <https://doi.10.22036/ABCR.2022.325691.1716>
- 27 Fatemeh Hosseini, S., Reza Talaie, M., Aghamiri, S., Khademi, M.H., Gholami, M. & Esfahany, M.N. (2017). Mathematical modeling of rapid temperature swing adsorption, the role of influencing parameters. *Separation and Purification Technology*, 183, 181–193. <https://doi.10.1016/j.seppur.2017.03.017>
- 28 Saranya, M., Srinivasan, L., Gopal Reddi, M.R., Gomathi, T., Sudha, P.N. & Anil, S. (2017). Adsorption Studies of Lead(II) from aqueous solution onto Nanochitosan / Polyurethane / Polypropylene glycol ternary blends. *International Journal of Biological Macromolecules*, 104(B), 436–4448. <https://doi.10.1016/j.ijbiomac.2017.06.004>
- 29 Haerifar, M. & Azizian S. (2012). Fractal-like adsorption kinetics at the solid/solution interface, *The Journal of Physical Chemistry C*, 116(24), 13111–13119. <https://doi.10.1021/jp301261h>
- 30 Zhuang, H., Zhong, Y. & Yang, L. (2020). Adsorption equilibrium and kinetics studies of divalent manganese from phosphoric acid solution by using cationic exchange resin. *Chinese Journal of Chemical Engineering*, 28(11), 2758–2770. <https://doi.10.1016/j.cjche.2020.07.029>
- 31 Ren W., Chang H., Mao T. & Tenga Y. (2019). Planarity effect of polychlorinated biphenyls adsorption by graphenenanomaterials, The influence of graphene characteristics, solution pH and temperature. *Chemical Engineering Journal*, 362, 160–168. <https://doi.10.1016/j.cej.2019.01.027>
- 32 Padmavathy, K.S., Madhu, G. & Haseena, P.V.A. (2016). Study on effects of ph, adsorbent dosage, time, initial concentration and adsorption isotherm study for the removal of hexavalent chromium (Cr (VI)) from wastewater by magnetite nanoparticles. *Procedia Technol*, 24, 585–594. <https://doi.10.1016/j.protcy.2016.05.127>
- 33 Gupta, N. & Sen, R. (2017). Kinetic and equilibrium modelling of Cu (II) adsorption from aqueous solution by chemically modified Groundnut husk (*Arachishypogaea*). *Journal of Environmental Chemical Engineering*, 5(5), 4274–4281. <https://doi.10.1016/j.jece.2017.07.048>
- 34 Xue, Y., Wu, S. & Zhou, M. (2013). Adsorption characterization of Cu(II) from aqueous solution onto basic oxygen furnace slag. *Chemical Engineering Journal*, 231, 355–364. <https://doi.10.1016/j.cej.2013.07.045>
- 35 Jiang, S., Huang, L., Nguyen, T.A.H., Sik, O.k. Y., Rudolph, V., Yang, H. & Zhang D. (2016). Copper and zinc adsorption by softwood and hardwood biochars under elevated sulphate-induced salinity and acidic pH conditions. *Chemosphere*, 142, 64–71. <https://doi.10.1016/j.chemosphere.2015.06.079>
- 36 Anayurt, R.A., Sari, A. & Tuzen, M. (2009). Equilibrium, thermodynamic and kinetic studies on biosorption of Pb (II) and Cd (II) from aqueous solution by macrofungus (*Lactarius scrobiculatus*) biomass. *Chemical Engineering Journal*, 151(1-3), 255–261. <https://doi.10.1016/j.cej.2009.03.002>
- 37 Esvandi, Z., Foroutan, R., Peighambari, S.J., Akbari, A. & Ramavandi, B. (2020). Uptake of anionic and cationic dyes from water using natural clay and clay/starch/MnFe₂O₄ magnetic nanocomposite. *Surfaces and Interfaces*, 21. <https://doi.10.1016/j.surfin.2020.100754>
- 38 Hu, C., Zhu, P., Cai, M., Hu, H. & Fu, Q. (2020). Comparative adsorption of Pb(II), Cu(II) and Cd(II) on chitosan saturated montmorillonite, Kinetic, thermodynamic and equilibrium studies. *Applied Clay Science*, 143, 320–326. <https://doi.10.1016/j.clay.2017.04.005>
- 39 Shafiee, M., Foroutan, R., Fouladi, K., Ahmadlouydarab, M., Ramavandi, B. & Sahebi, S. (2019). Application of oak powder/Fe₃O₄ magnetic composite in toxic metals removal from aqueous solutions. *Advanced Powder Technology*, 30(3), 544–554. <https://doi.10.1016/j.apt.2018.12.006>
- 40 Matsui, Y., Nakao, S., Sakamoto, A., Taniguchi, T., Pan L., Matsushita, T. & Shirasaki, N. (2016). Adsorption capacities of activated carbons for geosmin and 2-methylisoborneol vary with activated carbon particle size, Effects of adsorbent and adsorbate characteristics. *Water Research*, 85, 95–102. <https://doi.10.1016/j.watres.2015.08.017>
- 41 Sekar, M., Sakthi, V. & Rengaraj, S. (2004). Kinetics and equilibrium adsorption study of lead(II) onto activated carbon prepared from coconut shell. *Journal of Colloid and Interface Science*, 279(2), 307–313. <https://doi.10.1016/j.jcis.2004.06.042>
- 42 Ngah, W.W. & Hanafiah, M.A.K.M. (2008). Adsorption of copper on rubber (*Hevea brasiliensis*) leaf powder, Kinetic, equilibrium and thermodynamic studies. *Biochemical Engineering Journal*, 39(3), 521–530. <https://doi.10.1016/j.bej.2007.11.006>

- 43 Chouchane, T., Chouchane, S., Boukari, A. & Mesalhi, A. (2015). Adsorption of binary mixture «Lead Nickel» by kaolin. *Journal of Materials and Environmental Science*, 6(4), 924–941. ISSN: 2028-2508, CODEN: JMESCNC
- 44 Mustapha S., Shuaib D.T., Ndamitso M.M., Etsuyankpa M.B., Sumaila A., Mohammed U.M. & Nasirudeen M.B. (2019). Adsorption isotherm, kinetic and thermodynamic studies for the removal of Pb(II), Cd(II), Zn(II) and Cu(II) ions from aqueous solutions using Albizia lebeck pods. *Applied Water Science*, 9(6), 142. <https://doi.org/10.1007/s13201-019-1021-x>
- 45 Abdolali, A., Ngo, H.H., Guo, W., Zhou, J.L., Zhang, J., Liang, S., Chang, S.W., Nguyen, D.D. & Liu, Y. (2017). Application of a breakthrough biosorbent for removing heavy metals from synthetic and real wastewaters in a lab-scale continuous fixed-bed column. *Bioresource Technology*, 229, 78–87. <https://doi.org/10.1016/j.biortech.2017.01.016>
- 46 Freundlich, H.M.F. (1906). Over the adsorption in solution. *Journal of Physical Chemistry*, 57, 385–470. <https://doi.org/10.1515/zpch-1907-5723>
- 47 Langmuir, I. (1918). The adsorption of gases on plane surfaces of glass, mica and platinum. *Journal of the American Chemical Society*, 40, 1361–1403. <https://doi.org/10.1021/ja02242a004>
- 48 Temkin, M.I. (1940). Kinetics of ammonia synthesis on promoted iron catalysts. *Acta physiochim, URSS*, 12, 327–356.
- 49 Redlich, O. & Peterson, D.L. (1959). A Useful Adsorption Isotherm. *The Journal of Physical Chemistry*, 63(6), 1024–1024. <https://doi.org/10.1021/j150576a611>
- 50 Zahar, M.M.S., Kusin, F.M. & Muhammad, S.N. (2015). Adsorption of manganese in aqueous solution by steel slag. *Procedia Environmental Sciences*, 30, 145–150. <https://doi.org/10.1016/j.proenv.2015.10.026>
- 51 Mert Sivri, F., Hoda, N., Topuz, A., Budama Akpolat, L. & Eroğlu, E. (2022). Adsorption of dimethyl disulfide onto activated carbon cloth. *Turkish Journal of Chemistry*, 46, 859–868. <https://doi.org/10.55730/1300-0527.3374>
- 52 Maran, J.P., Sivakumar, V. & Sridhar, R. (2013). Thirugnanasambandham K. Development of model for barrier and optical properties of tapioca starch based edible films. *Carbohydrate Polymers*, 92(2), 1335–1347.
- 53 Gandhi, N., Sirisha, D. & Chandra Sekhar, K.B. (2016). Adsorption of Fluoride (F-) from Aqueous Solution by Using Pineapple (Ananas comosus) Peel and Orange (Citrus sinensis) Peel Powders. *International Journal of Environmental Bioremediation & Biodegradation*, 4(2), 55–67. <https://doi.org/10.12691/ijebb-4-2-4>
- 54 Ho, Y.S. & McKay, G. (1999). Pseudo-second order model for sorption processes. *Process Biochemistry*, 34(5), 451–465. [https://doi.org/10.1016/S0032-9592\(98\)00112-5](https://doi.org/10.1016/S0032-9592(98)00112-5)
- 55 Su, J., Lin, S., Chen, Z., Megharaj, M. & Naidu, R. (2011). Dechlorination of p-chlorophenol from aqueous solution using bentonite supported Fe/Pd nanoparticles, synthesis, characterization and kinetics, *Desalination*, 280(1–3), 167–73. <https://doi.org/10.1016/j.desal.2011.06.067>
- 56 Bhattacharya, A., Gupta, A., Kaur, A. & Malik, D. (2014). Efficacy of Acinetobacter sp. B9 for simultaneous removal of phenol and hexavalent chromium from co-contaminated system. *Applied Microbiology and Biotechnology*, 98, 9829–9841. <https://doi.org/10.1007/s00253-014-5910-5>
- 57 Alalwan, H.A., Mohammed, M.M., Sultan, A.J., Abbas, M.N., Ibrahim, T.A., Aljaafari H.A.S. & Alminshid A.A. (2021). Adsorption of methyl green stain from aqueous solutions using non-conventional adsorbent media, Isothermal kinetic and thermodynamic studies. *Bioresource Technology Reports*, 14. <https://doi.org/10.1016/j.biteb.2021.100680>.
- 58 Liu, T., Lawluy, Y., Shi, Y., Ighalo, J.O., He, Y., Zhang, Y. & Yap, P.-S (2022). Adsorption of cadmium and lead from aqueous solution using modified biochar, A review. *Journal of Environmental Chemical Engineering*, 10(1), 106502. <https://doi.org/10.1016/j.jece.2021.106502>
- 59 Chouchane T., Yahi M., Boukari A., Balaska A. & Chouchane S. (2016). Adsorption of the copper in solution by the kaolin. *Journal of Materials and Environmental Science*, 7(8), 2825–2842. ISSN: 2028-2508, CODEN: JMESCNC
- 60 Weber, Jr W.J. & Morriss, C. (1963). Kinetics of adsorption on carbon from solution. *Journal of the Sanitary Engineering Division*, 89(2), 31–60. <https://doi.org/10.1061/JSEDAI.0000430>
- 61 Ofomaja, A.E. (2010). Intraparticle diffusion process for lead(II) biosorption onto mansonia wood sawdust. *Bioresource Technology*, 101(15), 5868–5876. <https://doi.org/10.1016/j.biortech.2010.03.033>
- 62 Gao, R., Liu D., Huang, Y. & Li G. (2020). Preparation of diatomite-modified wood ceramics and the adsorption kinetics of tetracycline. *Ceramics International*, 46(12), 19799–19806. <https://doi.org/10.1016/j.ceramint.2020.05.014>
- 63 Cheung W.H., Szeto Y.S. & McKay G. (2007). Intraparticle diffusion processes during acid dye adsorption onto chitosan. *Bioresource Technology*, 98(15), 2897–2904. <https://doi.org/10.1016/j.biortech.2006.09.045>
- 64 Dehbi, A., Dehmani, Y., Omari, H., Lammini, A., Elazhari, K. & Abdallaoui, A. (2019). Hematite iron oxide nanoparticles (α -Fe₂O₃), synthesis and modelling adsorption of malachite green. *Journal of Environmental Chemical Engineering*, 8(1), 103394. <https://doi.org/10.1016/j.jece.2019.103394>
- 65 Fonseca-Correa, R.A., Giraldo, L. & Moreno-Piraján, J.C. (2019). Thermodynamic study of adsorption of nickel ions onto carbon aerogels. *Heliyon*, 5(6), e01789. <https://doi.org/10.1016/j.heliyon.2019.e01789>
- 66 Rajabzadeh, M., Aghaie, H. & Bahrami, H. (2020). Thermodynamic study of Iron (III) removing by the synthesized α -Alumina powder and evaluating the corresponding adsorption isotherm models using Response Surface Method. *Arabian Journal of Chemistry*, 13(2), 4254–4262. <https://doi.org/10.1016/j.arabjc.2019.07.006>
- 67 Kamaraj R. & Vasudevan S. (2016b). Facile one-pot synthesis of nano-zinc hydroxide by electro-dissolution of zinc as a sacrificial anode and the application for adsorption of Th⁴⁺, U⁴⁺, and Ce⁴⁺ from aqueous solution. *Research on Chemical Intermediates*, 42, 4077–4095. <https://doi.org/10.1007/s11164-015-2259-z>

68 Kalhori, E.M., Yetilmezsoy, K., Uygur, N., Zarrabi, M. & Shmeis, R.M.A. (2013). Modeling of adsorption of toxic chromium on natural and surface modified lightweight expanded clay aggregate (LECA). *Applied Surface Science*, 287, 428–442. <https://doi.10.1016/j.apsusc.2013.09.175>

69 Wang, S., Zhong, S., Zheng, X., Xiao, D., Zheng, L., Yang, Y., Zhang, H., Ai B. & Sheng, Z. (2021). Calcite modification of agricultural waste biochar highly improves the adsorption of Cu(II) from aqueous solutions. *Journal of Environmental Chemical Engineering*, 9(5). <https://doi.10.1016/j.jece.2021.106215>

Information about authors*

Chouchane, Toufik (*corresponding author*) — Research Director and research team leader, Leading researcher, Research Center in Industrial Technologies CRTI, P.O. Box 64, Cheraga 16014 Algiers Algeria; e-mail: chouchane_toufik@yahoo.fr; t.chouchane@crti.dz; <https://orcid.org/0000-0001-8979-0667>

Boukari, Atmane — Searcher, Research Center in Industrial Technologies CRTI, P.O. Box 64, Cheraga 16014 Algiers Algeria; e-mail: a.boukari@crti.dz;

Khiredine, Ouahida — Searcher, Research Center in Industrial Technologies CRTI, P.O. Box 64, Cheraga 16014 Algiers Algeria; e-mail: o.khiredine@crti.dz; <https://orcid.org/0000-0001-6890-5744>

Chibani, Sana — Searcher, Research Center in Industrial Technologies CRTI, P.O. Box 64, Cheraga 16014 Algiers Algeria; e-mail: s.chibani@crti.dz; <https://orcid.org/0000-0002-0339-8320>

Chouchane, Sabiha — Professor, Faculty of Sciences, Badji Mokhtar Annaba University, Annaba Algeria; e-mail: chouchsam01@yahoo.fr; <https://orcid.org/0000-0003-2587-4372>

*The author's name is presented in the order: *Last Name, First and Middle Names*